The quantity (A) is defined by expression (4). As an example of the results obtained from expression (7), a set of calculations was made for the condition of $T_R = 177°K$ and for T_v values of 177° and 2700°K. The results are given in Table 2.

It is noted that there is very little change in the relative population of the excited ionized state of N_2^+ for each T_v considered. There is a slight population shift from the lower quantum states to the upper quantum states for the 2700°K T_v case. Since a relatively large change in the T_v does not significantly change the relative population distribution of the rotational energy states of the zero vibrational energy level of $N_2^+B^2\Sigma_u^+$, only a small difference will exist between the results of Eqs. (1) and (6). Of course, the total population of the zero vibrational energy level of $N_2^+B^2\Sigma^+{}_u$ does change with T_v as shown in Fig. 1.

Muntz[1,2] noted that the rotational energy-state population distribution for $v' = 0$ energy level of $N_2^+B^2\Sigma_u^+$ was not a significantly strong function of T_v because of the particular distribution of Franck-Condon factors. This point was examined further by comparing the relative population variation of $v' = 0$, 1, and 2 of $N_2^+B^2\Sigma_u^+$ for $T_R = 25°K$ and $T_v = 25°K$ and 4000°K. The increase of T_v from 25° to 4000°K resulted in a shift of population from the lower rotational quantum states to the upper quantum states. The degree of population shift increased with the vibrational quantum number. For example, the relative change in the rotational quantum state $K' = 6$ of $v' = 0$, 1, and 2 was approximately 0.1, 1.8, and 3.9%, respectively.

In summary, Eq. (6) provides a single equation which is applicable for a broad T_v range. A comparison of results obtained with Eqs. (1) and (6) applied to specific cases of transition from the $v' = 0$ level of $N_2^+B^2\Sigma_u^+$ shows that Eq. (1) may be applied for a range of T_v values up to 2700°K without introducing a significant error in the resultant T_R values. It was shown that this was because the population distribution of the $v' = 0$ level of $N_2^+B^2\Sigma_u^+$ was not a strong function of T_v. The application of Eq. (1) to transitions from vibrational energy states other than $v' = 0$ of $N_2^+B^2\Sigma_u^+$ must be done with care since the population shift is greater for higher T_v's.

Table 2 Relative population of the zero vibrational level of $N_2^+B^2\Sigma_u^+$ for 177°K rotational temperature and 177°K and 2700°K vibrational temperature

	T_v	
K'	177°K	2700°K
1	0.06102	0.06100
2	0.04776	0.04775
3	0.12175	0.12173
4	0.06906	0.06904
5	0.14434	0.14433
6	0.07069	0.07068
7	0.13101	0.13101
8	0.05779	0.05779
9	0.09744	0.09746
10	0.03937	0.03938
11	0.06110	0.06112
12	0.02280	0.02281
13	0.03277	0.03279
14	0.01135	0.01136
15	0.01516	0.01517
16	0.00489	0.00489
17	0.00608	0.00609
18	0.00183	0.00183
19	0.00212	0.00213
20	0.00060	0.00060
21	0.00065	0.00065
22	0.00017	0.00017
23	0.00017	0.00017
24	0.00004	0.00004

References

[1] Muntz, E. P., "Static Temperature Measurements in a Flowing Gas," *The Physics of Fluids*, Vol. 5, No. 1, Jan. 1962, pp. 80–90.

[2] Muntz, E. P., "Measurement of Rotational Temperature, Vibrational Temperature, and Molecular Concentration, in Non-Radiating Flows of Low Density Nitrogen," UTIA Rept. 71, April 1961, University of Toronto, Toronto, Canada.

[3] Petrie, S. L., "Electron Beam Diagnostics," *AIAA Journal*, Vol. 4, No. 9, Sept. 1966, pp. 1679–1680.

[4] Sebacher, D. I. and Duckett, R. J., "A Spectrographic Analysis of a 1-Foot Hypersonic-Arc-Tunnel Airstream Using an Electron Beam Probe," TR R-214, Dec. 1964, NASA.

[5] Petrie, S. L., Pierce, G. A., and Fishburne, E. S., "Analysis of the Thermo-Chemical State of an Expanded Air Plasma," AFFDL-TR-64-191, Aug. 1965, U.S. Air Force Flight Dynamics Lab.

[6] Hunter, W. W., Jr., "Investigation of Temperature Measurements in 300° to 1100°K Low-Density Air Using an Electron Beam Probe," TN D-4500, May 1968, NASA.

[7] Herzberg, G., *Molecular Spectra and Molecular Structure*, 2nd ed., Vol. 1, D. Van Nostrand, Princeton, N.J., 1950.

[8] Clark, F. L., Ellison, J. C., and Johnson, C. B., "Recent Work in Flow Evaluation and Techniques of Operations for the Langley Hypersonic Nitrogen Facility," *Fifth Hypervelocity Techniques Symposium, Advance Experimental Technique for Study of Hypervelocity Flight*, Vol. 1, 1967, pp. 347–373.

Problem of the Annular Plate, Simply Supported and Loaded with an Eccentric Concentrated Force

R. Amon*
University of Illinois, Chicago, Ill.

AND

O. E. Widera†
University of Stuttgart, Stuttgart, West Germany

AND

R. G. Ahrens‡
Chicago, Ill.

Introduction

THE subject of this paper is the determination of the deflection function for the annular plate, simply supported at both edges, and loaded with an eccentric concentrated force. In a previous paper,[1] the problem of the clamped annular plate was discussed. The actual boundary conditions probably vary somewhere between these two cases. According to the Poisson-Kirchoff theory of bending of thin plates,[2] the deflection w is a solution of the equation

$$\nabla^4 w = q/D \tag{1}$$

where ∇^4 is the biharmonic operator, q is the transverse load intensity, and D the plate flexural rigidity. For a problem of the type considered, the solution can be expressed in the form

$$w = w_S + w_R \tag{2}$$

Here, w_S represents the singular solution state the w_R the

Received October 2, 1969; revision received December 22, 1969.

* Associate Professor of Structural Engineering.

† Visiting Professor (on leave of absence from University of Illinois, Chicago).

‡ Structural Engineer.

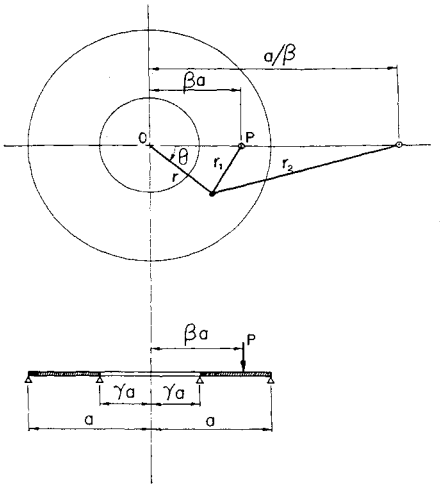

Fig. 1 Simply supported annular plate.

solution of $\nabla^4 w = 0$, so chosen that the boundary conditions on w are satisfied.

The related problem of the circular plate, simply supported at the edges and under a concentrated force, was obtained by Reissner[3] in 1935 in integral form. In 1952, Washizu[4] obtained the same solution in series form,

$$w = \frac{Pa^2}{8\pi D}\left\{\rho_1^2 \log\left(\frac{\rho_1}{\beta\rho_2}\right) + \frac{1}{2}(1-\beta^2)(1-\rho^2)\times \left[\frac{3+\nu}{1+\nu} + 4\sum_{n=1}^{\infty}\frac{(\beta\rho)^n \cos n\theta}{1+\nu+2n}\right]\right\} \quad (3)$$

where $\rho = r/a$, and (see Fig. 1)

$$\begin{aligned} \rho_1^2 &= \rho^2 + \beta^2 - 2\beta\rho\cos\theta \\ \beta^2\rho_2^2 &= \rho^2\beta^2 + 1 - 2\beta\rho\cos\theta \end{aligned} \quad (4)$$

The first term in Eq. (3) is seen to contain the proper singularity for a concentrated force, this being the term $(Pa^2/8\pi D) \times \rho_1^2 \log\rho_1$. A comprehensive review of problems dealing with concentrated forces on circular plates can be found in the paper by Dundurs and Lee.[5] Their method of solution is used in the following analysis.

Solution

The plate takes the form of an annulus with an outer radius a and an inner radius γa, supported at both edges and loaded with a single concentrated force P located at a distance βa from the center 0 (see Fig. 1). For the singular solution we take Washizu's solution Eq. (3) for the circular plate. The regular solution is assumed to take the form

$$w_R = \frac{Pa^2}{8\pi D}[A_0 + B_0\log\rho + C_0\rho^2 + D_0\rho^2\log\rho + (A_1\rho + B_1\rho^{-1} + C_1\rho^3 + D_1\rho\log\rho)\cos\theta + \sum_{n=2}^{\infty}\times (A_n\rho^n + B_n\rho^{-n} + C_n\rho^{n+2} + D_n\rho^{-n+2})\cos n\theta] \quad (5)$$

The boundary conditions of the problem are

$$w = M_r = 0 \ (\rho = \gamma) \quad (6)$$

$$w_R = M_r(w_R) = 0 \ (\rho = 1) \quad (7)$$

Here,

$$M_r = -D\left[\frac{\partial^2 w}{\partial r^2} + \nu\left(\frac{1}{r}\frac{\partial w}{\partial r} + \frac{1}{r^2}\frac{\partial^2 w}{\partial\theta^2}\right)\right] \quad (8)$$

In order to satisfy the conditions on the radial moment, it will be necessary to expand the expression $\rho_1^2\log(\rho_1/\beta\rho_2)$ for $\gamma \le \rho < \beta$ in terms of cosine multiples of θ. The result is given in Ref. 1. The contribution to the bending moment of the singular solution state can then be expressed as

$$M_r(w_s) = -\frac{P}{8\pi D}\left\{2(1-\nu)\log\beta + (\beta^2-1)(1-\nu) + \cos\theta\left[\rho(1-\beta^2)\left((3+\nu)\left(\beta - \frac{1}{\beta}\right) - 4\beta\right)\right] + \sum_{n=2}^{\infty}\cos n\theta \times \left\langle \rho^n(n+1)[(n+2) - \nu(n-2)]\left[\left(\beta^n - \frac{1}{\beta^n}\right)\frac{1}{n} - \left(\beta^{n+1} - \frac{1}{\beta^{n+1}}\right)\frac{\beta}{n+1} - \frac{2(1-\beta^2)\beta^n}{2n+1+\nu}\right] + \rho^{n-2}n \times (n-1)(1-\nu)\left[\left(\beta^n - \frac{1}{\beta^n}\right)\frac{\beta^2}{n} - \left(\beta^{n-1} - \frac{1}{\beta^{n-1}}\right)\frac{\beta}{n-1} + \frac{2(1-\beta^2)\beta^2}{2n+1+\nu}\right]\right\rangle\right\} \quad (9)$$

Satisfaction of boundary conditions Eqs. (6) and (7) yields the simultaneous equations required to find the integration constants A, B, C, and D. The result is

$$A_0 + C_0 = 0 \quad (10a)$$

$$B_0(1-\nu) - 2C_0(1+\nu) - D_0(3+\nu) = 0 \quad (10b)$$

$$A_0 + B_0\log\gamma + C_0\gamma^2 + D_0\gamma^2\log\gamma + \beta^2\log\beta + \frac{1}{2}(1-\beta^2)\left(\frac{3+\nu}{1+\nu}\right) + \gamma^2\left[\log\beta + (1-\beta^2)\times\left\{1 - \frac{1}{2}\left(\frac{3+\nu}{1-\nu}\right)\right\}\right] = 0 \quad (10c)$$

$$B_0\gamma^{-2}(1-\nu) + 2C_0(1+\nu) + D_0[2\log\gamma(1+\nu) + (3+\nu)] + 2(1+\nu)\log\beta + (\beta^2-1)(1-\nu) = 0 \quad (10d)$$

$$A_1 + B_1 + C_1 = 0 \quad (11a)$$

$$2B_1(1-\nu) + 2C_1(3+\nu) + D_1(1+\nu) = 0 \quad (11b)$$

$$A_1\gamma^2 + B_1 + C_1\gamma^4 + D_1\gamma^2\log\gamma - \gamma^2\left[2\beta\log\beta - \beta(\beta^2-1)\left(\frac{1+\nu}{3+\nu}\right)\right] - \gamma^4(\beta^2-1)\times \frac{1}{2}\left[\frac{(3+\nu)(\beta^2-1) - 4\beta^2}{\beta(3+\nu)}\right] = 0 \quad (11c)$$

$$2B_1\gamma^{-2}(1-\nu) + 2C_1\gamma^2(3+\nu) + D_1(1+\nu) - \gamma^2(\beta^2-1)\left[(3+\nu)\left(\beta - \frac{1}{\beta}\right) - 4\beta\right] = 0 \quad (11d)$$

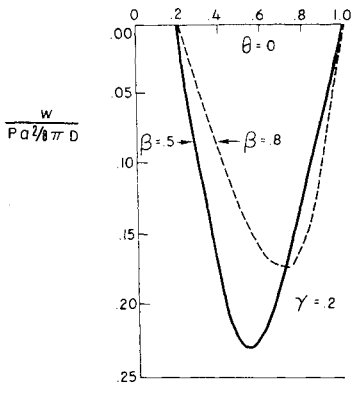

Fig. 2 Deflection along the load carrying radius.

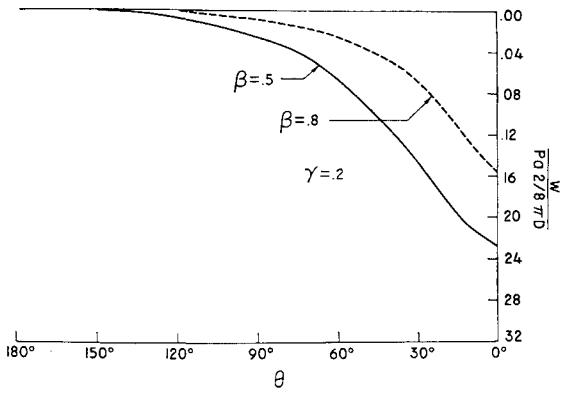

Fig. 3 Deflection along the circle of βa radius.

$$A_n + B_n + C_n + D_n = 0 \quad (12a)$$

$$A_n n(n-1)(1-\nu) + B_n n(n+1)(1-\nu) + C_n(n+1)[(n+2) - \nu(n-2)] + D_n \times (n-1)[(n-2) - \nu(n+2)] = 0 \quad (12b)$$

$$A_n(\gamma^2)^n + B_n + C_n(\gamma^2)^{n+1} + D_n\gamma^2 + (\gamma^2)^n \left[\frac{1}{\beta^n}\langle(\beta^2)^n - 1\rangle \times \frac{(\gamma^2+\beta^2)}{n} - \frac{1}{\beta^{n+1}}\langle(\beta^2)^{n+1} - 1\rangle \frac{\beta\gamma^2}{n+1} - \frac{1}{\beta^{n-1}}\langle(\beta^2)^{n-1} - 1\rangle \frac{\beta}{n-1} + \frac{2(1-\beta^2)\beta^n}{2n+1+\nu} \times (1-\nu^2)\right] = 0 \quad (12c)$$

$$A_n(\gamma^2)^{n-1}n(n-1)(1-\nu) + B_n\gamma^{-2}n(n+1)(1-\nu) + C_n(\gamma^2)^n(n+1)[(n+2) - \nu(n-2)] + D_n(n-1)[(n-2) - \nu(n+2)] + (\gamma^2)^n\left[(n+1)\langle(n+2) - \nu(n-2)\rangle\left(\frac{1}{\beta^n}\langle(\beta^2)^n - 1\rangle\frac{1}{n} - \frac{1}{\beta^{n+1}}\langle(\beta^2)^{n+1} - 1\rangle\frac{\beta}{n+1} - \frac{2(1-\beta^2)\beta^3}{2n+1+\nu}\right) + n\langle(n-1)(1-\nu)\rangle\left(\frac{1}{\beta^n}\langle(\beta^2)^n - 1\rangle \times \frac{\beta^2}{n} - \frac{1}{\beta^{n-1}}\langle(\beta^2)^{n-1} - 1\rangle \frac{\beta}{n-1} + \frac{2(1-\beta^2)\beta^3}{2n+1+\nu}\right)\right] = 0 \quad (12d)$$

Results

In Figs. 2 and 3 the deflection along a radial line $w = w(\rho)$ and along a circumferential line $w = w(\theta)$, respectively, have been plotted for $\gamma = 0.2$ and for $\beta = 0.5, 0.8$. It is seen that the deflection of the region diametrically opposite to the point of application of load is, for all practical purposes, nil, and that the width of this area is a sector of about 90°. It can thus be inferred that in this region the stress resultants and stresses are very small.

A comparison of the result obtained here with those of Ref. 1 for the clamped plate indicates that the deflection and the deflection zone are twice as large as for the clamped case.

References

[1] Amon, R. and Widera, O. E., "Clamped Annular Plate under a Concentrated Source," *AIAA Journal*, Vol. 7, No. 1, Jan. 1969, pp. 151–153.

[2] Timoshenko, S. and Woinowsky-Krieger, S., *Theory of Plates and Shells*, McGraw-Hill, New York, 1959.

[3] Reissner, E., "Über die Biegung der Kreisplatte mit exzentrischer Einzellast," *Mathematische Annalen*, Vol. 3, 1935, pp. 777–780.

[4] Washizu, K., "On the Bending of Isotropic Plates," *Transactions of the Japan Society of Mechanical Engineers*, Vol. 18, 1952, pp. 41–47.

[5] Dundurs, J. and Lee, T. M., "Flexure by a Concentrated Force of the Infinite Plate on a Circular Support," *Journal of Applied Mechanics*, Vol. 30, 1963, pp. 225–231.

A Planview Shadowgraph Technique for Boundary-Layer Visualization

ENRIQUE J. KLEIN*
NASA Ames Research Center, Moffett Field, Calif.

As part of a study on the formation and growth of disturbances generated by spark discharges into a laminar boundary layer,[1] an optical arrangement was devised to observe such disturbances viewed against the surface of the model rather than across its edge as in conventional systems. This was achieved by using a double-pass focused shadowgraph system, incorporating in the wind-tunnel test section a plane mirror that served simultaneously as a flat-plate model. Tests were made in the Ames 1- by 3-ft supersonic wind tunnel.

The optical arrangement is shown schematically in the diagram of Fig. 1. It consisted of a spark gap with interchangeable apertures, a beam splitter, a first surface spherical mirror of 18-in. diam and 120-in. focal length, a flat mirror model, as well as a focusing lens of 52.5-in. focal length, a shutter and aperture, a camera box of adjustable length, and a 4- by 5-in. film holder, all mounted on an optical bench. In practice, the beam splitter was replaced by a first surface mirror to increase the lighting efficiency. It was set at an angle of 45° and slightly off axis to avoid intercepting the light rays returning from the test section. The optical paths from the spark gap aperture and the focusing lens to the spherical mirror were both set at 120 in., the focal distance of the mirror. The focal length of the focusing lens and the length of the camera box were calculated to obtain an image reduction of 3:1 with the model surface in focus. The model was a flat plate with a 6- by 10-in. surface and a sharp leading edge. It was made of stress-relieved mild steel, coated with nickel to obtain an appropriate hardness, and polished to $\lambda_D/4$ flatness. This surface later was coated with a layer of vacuum-deposited aluminum and a protective layer of silicon monoxide. A grid of 0.5-in. spacing was painted on this surface for reference.

In this optical system, the light from the spark gap first reaches the spherical mirror, where it is reflected as a parallel beam of light to the test section. At the mirror model, it is reflected back to the spherical mirror and from there through the focusing lens, shutter, and aperture to the film. To obtain a shadowgraph of the density variations in the boundary layer on the mirror model, it becomes necessary to focus the system not on the surface of the mirror model but on a plane closer to the spherical mirror. Ideally, focusing on the inside surface of the wind-tunnel window would eliminate the image of the density gradients of the window boundary layer while permitting a clear view of the density gradients of the model boundary layer.

Received December 15, 1969. This investigation was accomplished during the author's tenure of a National Research Council Postdoctoral Research Associateship supported by NASA. The author is indebted to G. B. Schubauer of the National Bureau of Standards, as the concept for this technique originated in a discussion with him. I also would like to express my appreciation to R. M. Brown, who carried out the analysis for the optical system.

* National Research Council—Research Associate. Associate Fellow AIAA.